Geophys. J. Int. (2002) **148,** 303–312

Identifying elements of the plumbing system beneath Kilauea Volcano, Hawaii, from the source locations of very-long-period signals

Javier Almendros,[1,*] Bernard Chouet,[1] Phillip Dawson[1] and Timothy Bond[2]
[1] *U.S. Geological Survey, Menlo Park, CA, USA*
[2] *Imperial College, UK*

Accepted 2001 November 6. Received 2001 November 6; in original form 2001 June 5

SUMMARY

We analyzed 16 seismic events recorded by the Hawaiian broad-band seismic network at Kilauea Volcano during the period September 9–26, 1999. Two distinct types of event are identified based on their spectral content, very-long-period (VLP) waveform, amplitude decay pattern and particle motion. We locate the VLP signals with a method based on analyses of semblance and particle motion. Different source regions are identified for the two event types. One source region is located at depths of ∼1 km beneath the northeast edge of the Halemaumau pit crater. A second region is located at depths of ∼8 km below the northwest quadrant of Kilauea caldera. Our study represents the first time that such deep sources have been identified in VLP data at Kilauea. This discovery opens the possibility of obtaining a detailed image of the location and geometry of the magma plumbing system beneath this volcano based on source locations and moment tensor inversions of VLP signals recorded by a permanent, large-aperture broad-band network.

Key words: Kilauea volcano, very-long-period events, volcano seismology.

1 INTRODUCTION

A significant factor in our understanding of volcanic behavior is knowledge of the extent and geometry of the underlying magma conduits. Attempts to locate magma conduits have been made at several volcanoes based on hypocentre locations of volcano-tectonic (VT) earthquakes induced in the surrounding medium by magma movements (Ryan *et al.* 1981; Klein *et al.* 1987; Lahr *et al.* 1994). Such studies, however, map stress concentrations distributed over a large volume surrounding magma conduits in a medium whose structural properties are generally poorly known. Studies of VT earthquakes can only roughly delimit the boundaries of the volcanic plumbing system and do not yield precise information about the location and geometry of magma conduits. A more useful approach for this purpose is to rely on long-period (LP) and very-long-period (VLP) signals caused by fluids moving in volcanic conduits. Although alternative models have been proposed (e.g. Julian 1994), the prevailing theory used to explain the origin of these types of signals assumes that LP signals with periods in the range 0.2–2 s originate in acoustic resonances of fluid-filled conduits triggered by pressure transients (Chouet 1996a), while VLP signals with dominant periods in the range of a few tens of seconds are assumed to be linked to mass movements and to represent inertial forces resulting from perturbations in the flow of magma and gases through conduits (Uhira & Takeo 1994; Chouet 1996b; Ohminato *et al.* 1998; Nishimura *et al.* 2000). Accordingly, source locations of LP and VLP signals arguably represent the most accurate approach to mapping plumbing systems beneath volcanoes. The wavelengths of VLP signals are in the range of tens to hundreds of kilometres, which greatly facilitates their analysis. Moment tensor inversions of VLP waveforms (Uhira & Takeo 1994; Ohminato *et al.* 1998; Legrand *et al.* 2000; Nishimura *et al.* 2000) yield information about the source mechanisms, thus shedding light on the source geometry and source dynamics of these events.

As a result of an increased use of broad-band seismometers on volcanoes we now understand that VLP signals are common phenomena which are intimately related to the dynamics of magma and/or hydrothermal fluid transport (Aster *et al.* 2000). VLP signals have been documented in volcanic areas all over the world, including Kilauea (Chouet & Dawson 1997; Ohminato *et al.* 1998), Aso (Kaneshima *et al.* 1996; Kawakatsu *et al.* 2000; Legrand *et al.* 2000), Iwate (Nishimura *et al.* 2000), Miyakejima (Kumagai *et al.* 2001), Sakurajima (Uhira & Takeo 1994), Stromboli (Falsaperla *et al.* 1994; Neuberg *et al.* 1994; Wassermann 1997; Chouet *et al.* 1999), Merapi (Hidayat *et al.* 2000),

*Now at: Instituto Andaluz de Geofisica, University of Granada, 18071 Granada, Spain.

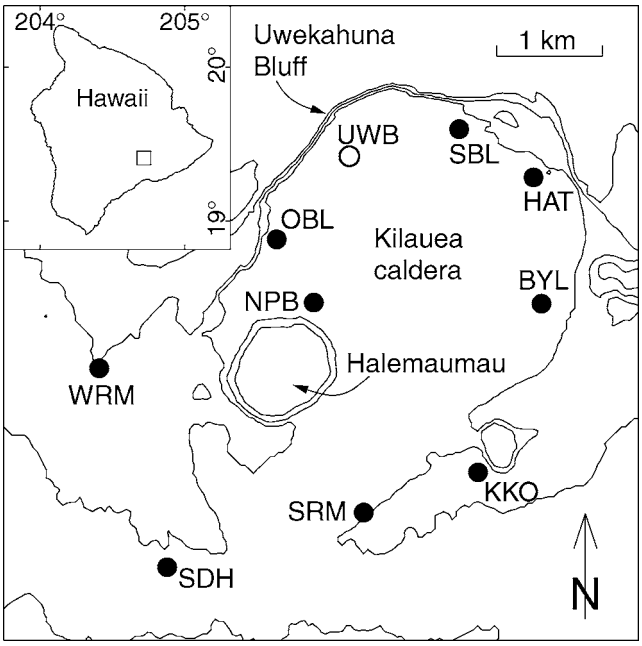

Figure 1. Map of Kilauea caldera showing the configuration of the broad-band seismic instruments used in the present paper (solid black circles). Station UWB (open circle) was inoperative during the time of the study. The inset shows the position of the caldera on the island of Hawaii.

Popocatepetl (Arciniega-Ceballos *et al.* 1999), Long Valley (Hill *et al.* in preparation 2001) and Erebus (Rowe *et al.* 1998). Some of these studies report on source locations of individual VLP signals. In this paper, we demonstrate the feasibility of obtaining a detailed image of the plumbing system at Kilauea Volcano by direct observation of VLP signals generated in two different segments of the conduit or conduits.

2 INSTRUMENTS

The data were recorded by the USGS permanent broad-band seismic network which has been operating at Kilauea Volcano since 1994 (Dawson *et al.* 1998). In its present configuration, stable since February 1998, the network has an aperture of 5 km and features 10 three-component broad-band stations (Fig. 1). All channels are sampled at 100 samples per second. Stations HAT, NPB, OBL, SRM, UWB, and WRM are equipped with Guralp CMG-40T seismometers with a flat response from 0.02 to 60 s; stations BYL, KKO, and SBL are equipped with Guralp CMG-3T seismometers with a flat response from 0.02 to 100 s; and station SDH features a Streckheisen STS-2 seismometer with a flat response from 0.02 to 120 s. In September 1999, however, station UWB was inoperative due to a failure of its digital telemetry unit. Therefore, the network used in the present analysis consists of 9 stations only.

3 DATA DESCRIPTION

Our analysis focuses on seismic activity that occurred between September 9 and 26, 1999. During this interval, coincident with Pause 26 in the ongoing Puu Oo eruption (Heliker *et al.* 1998), only the Upper East Rift was active with the occurrence of a seismic swarm and high-amplitude tremor on September 12. The Kilauea summit region was seismically quiet for most of the time. Apart from a few teleseisms and a background noise dominated by oceanic microseismic components, only a few tens of volcano-related seismic events, emergent in character and with durations near 60 s, were detected. We selected 16 of the latter events, characterized by high signal-to-noise ratios, for analysis. The times of occurrence of these events are listed in Table 1. To facilitate the identification of VLP signals and minimize the effects of microseismic noise, which usually peaks between 2 and 7 s at Kilauea (Dawson *et al.* 1998), all traces are bandpass filtered between 8 and 60 s.

Fig. 2 illustrates the frequency content of two of the analyzed events. Event 1 (Fig. 2a) shows energy concentrated in the VLP band, and Event 16 (Fig. 2b), which is more energetic, contains energy distributed over a wider frequency band extending over the entire bandwidth of the broad-band sensor and probably beyond this bandwidth as well. Several observations of high-frequency components riding on VLP signals have been reported previously (Dawson *et al.* 1998; Chouet *et al.* 1999; Arciniega-Ceballos *et al.* 1999; Hidayat *et al.* 2000; Hill *et al.* in preparation 2001). The short-wavelength components may be generated by the same source that produces the VLP signals or indirectly by excitation of secondary cracks located away from the primary source (Hill *et al.* in preparation 2001). The usually emergent character of the high-frequency waves makes the task of locating their source rather difficult. The combined use of a broad-band network and dense seismic arrays may be required to fully document the characteristics of such signals.

Apart from their characteristic frequency content, other differences between Events 1 and 16 are evident. Fig. 3 shows particle motion and amplitude decay patterns recorded by the network for these two events. For both events, particle motion is highly rectilinear at all stations. Similar observations reported at other volcanoes (Ohminato *et al.* 1998; Dawson *et al.* 1998; Chouet *et al.* 1999; Arciniega-Ceballos *et al.*

Table 1. Times and source locations obtained for the events selected for this study.

Type	Event	Time	East* (km)	North* (km)	Depth* (km)	Semblance†
	1	99/09/14 21:51:42	−0.28[**0.16**]0.48	−0.16[**0.24**]0.60	0.64[**1.00**]1.52	0.94
	2	99/09/17 11:56:55	−0.12[**0.28**]0.68	−0.08[**0.28**]0.64	0.56[**1.00**]1.40	0.71
	3	99/09/19 00:30:43	−0.36[−**0.08**]0.28	−0.20[**0.16**]0.52	0.52[**0.92**]1.36	0.81
I	4	99/09/25 05:31:45	−0.44[−**0.08**]0.28	−0.24[**0.20**]0.56	0.52[**0.92**]1.40	0.81
	5	99/09/25 12:56:18	−0.48[−**0.12**]0.24	0.08[**0.48**]0.80	0.52[**0.88**]1.40	0.64
	6	99/09/26 07:39:58	−0.28[**0.08**]0.44	0.12[**0.48**]0.80	0.60[**1.00**]1.52	0.83
	7	99/09/26 07:48:06	−0.08[**0.24**]0.64	0.00[**0.40**]0.72	0.56[**0.96**]1.48	0.74
	8	99/09/10 20:20:42	−0.8[**0.0**]0.8	0.6[**1.2**]2.2	5.4[**7.4**]∞	0.95
	9	99/09/12 06:56:54	−0.8[**0.0**]0.8	0.6[**1.4**]2.4	5.4[**7.8**]∞	0.97
	10	99/09/13 13:08:02	−0.6[**0.2**]1.0	0.8[**1.4**]2.6	5.4[**7.6**]∞	0.94
	11	99/09/15 09:20:24	−0.6[**0.2**]1.0	1.0[**1.6**]2.8	5.6[**8.0**]∞	0.96
II	12	99/09/15 21:53:35	−1.0[−**0.2**]0.8	0.8[**1.6**]2.6	5.8[**9.0**]∞	0.97
	13	99/09/17 08:33:23	−1.0[**0.0**]0.8	0.8[**1.4**]2.6	5.6[**7.8**]∞	0.96
	14	99/09/17 10:31:08	−0.2[**0.4**]1.0	1.0[**1.6**]2.4	4.4[**6.2**]8.8	0.89
	15	99/09/19 15:08:11	−0.8[**0.2**]1.0	1.0[**1.8**]3.0	5.8[**8.0**]∞	0.95
	16	99/09/21 10:28:25	−1.2[−**0.2**]0.6	1.0[**1.8**]3.0	5.8[**8.4**]∞	0.96

*Expressed as: lower error limit [**central value**] upper error limit.
†Maximum of the average semblance distribution for the event.

1999; Kawakatsu *et al.* 2000) suggest that the long wavelengths of these signals mainly reflect the near-field components of the source wavefield (Legrand *et al.* 2000). Particle motion for Event 1 shows distinct incidence angles and generally points to a shallow source below the center of the network, while particle motion for Event 16 is almost vertical, consistent with a deeper source.

Differences in signal amplitudes across the network are also obvious in Fig. 3. For Event 1, we observe amplitude variations from station to station ranging up to a factor of 10. The most energetic signal is recorded at station NPB (see Fig. 1), pointing to a shallow source located approximately beneath the center of the network. For Event 16, however, all stations display roughly the same amplitude, again consistent with a much deeper source.

The characteristics of the other 14 events are similar to either one or the other of the two events described above (Fig. 4). We classify events similar to Event 1 as Type I events (events 1 to 7) and events similar to Event 16 as Type II events (events 8 to 16) (see Table 1).

4 SOURCE LOCATION METHOD

The location method is specifically designed for the location of isotropic sources with a network of three-component seismometers (Kawakatsu *et al.* 2000). The method is based on estimations of semblance, a measure of the similarities in multichannel data as first discussed by Neidel & Tarner (1971), weighted according to the rectilinearity of the particle motions. Denoting $\mathbf{U}_i$ as the ground motion recorded at receiver i, the definition of semblance according to Kawakatsu *et al.* (2000), is

$$S_K = \frac{\sum_{j=1}^{M}\left(\left(\sum_{i=1}^{N}\mathbf{U}_i^p(\tau_i+j\Delta t)\right)^2 - N\sum_{i=1}^{N}\left(\mathbf{U}_i^v(\tau_i+j\Delta t)^2+\mathbf{U}_i^h(\tau_i+j\Delta t)^2\right)\right)}{N\sum_{j=1}^{M}\sum_{i=1}^{N}\left(\mathbf{U}_i^p(\tau_i+j\Delta t)^2+\mathbf{U}_i^v(\tau_i+j\Delta t)^2+\mathbf{U}_i^h(\tau_i+j\Delta t)^2\right)}, \tag{1}$$

where the superscript p represents the source–receiver direction, and the superscripts v and h represent two mutually perpendicular directions normal to the p direction, τ_i is the start time of the analysis window at receiver i, N is the number of receivers in the network, M is the number of samples in the window, and Δt is the sampling interval. As Kawakatsu *et al.* (2000) perform a normalization of each seismogram by the 3-D RMS amplitude of the signal at each receiver before applying eq. (1), we can simplify their definition and use a modified semblance given by

$$S = \frac{S_K+1}{2} = \frac{1}{2MN^2}\sum_{j=1}^{M}\left[\left(\sum_{i=1}^{N}\frac{\mathbf{U}_i^p(\tau_i+j\Delta t)}{\sigma_i}\right)^2 + N\sum_{i=1}^{N}\left(\frac{\mathbf{U}_i^p(\tau_i+j\Delta t)}{\sigma_i}\right)^2\right], \tag{2}$$

where σ_i is the three-component RMS of the ground motion at receiver i, defined as

$$\sigma_i = \sqrt{\frac{1}{M}\sum_{j=1}^{M}|\mathbf{U}_i(\tau_i+j\Delta t)|^2}. \tag{3}$$

The application of the method consists in finding the set of times τ_i that yields the maximum semblance. In the case of a seismic source, arrival times can be expressed as

$$\tau_i(\mathbf{r}) = t_0 + \tau_i'(\mathbf{r}), \tag{4}$$

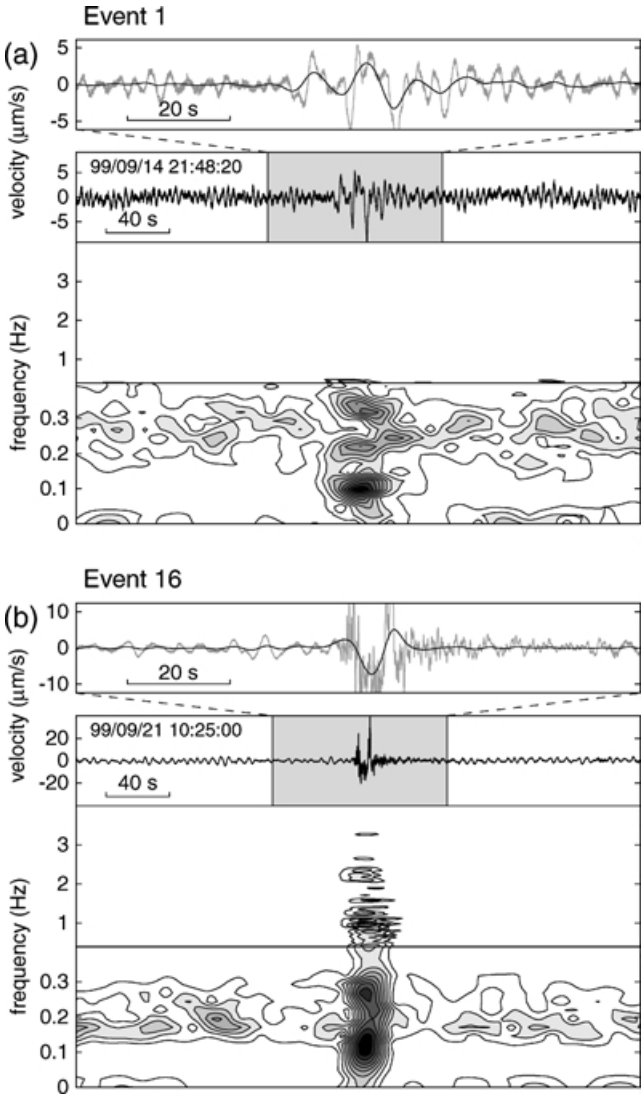

Figure 2. (a) From top to bottom, detail of filtered (black) overlaid on raw (grey) vertical ground velocity recorded at station NPB for Event 1 (see Table 1) for the shaded interval shown below; raw vertical velocity and corresponding spectrogram obtained from a 40 s long window sliding in increments of 2 s along the trace. The frequency axis is partitioned into two linear segments—ranging from 0 to 0.4 Hz and from 0.4 to 4 Hz, respectively—to emphasize the low-frequency content of the signal but still show frequencies up to 4 Hz. In this case, there is little energy visible in the higher frequency band. (b) The same for Event 16 (see Table 1). In this case, the frequency content extends well into the higher frequency band.

where t_0 represents the event origin time, and τ_i' is the traveltime to the ith receiver from a source located at $\mathbf{r}$. The calculated travel times depend on the source position, the receiver position and our selection of the velocity model used to represent the medium. Because of the very long wavelengths involved, a homogeneous medium is adequate for our purpose. In such a model, the maximum semblance is reached when the travel times τ_i' satisfy the relation

$$\tau_i'(\mathbf{r}) = \frac{|\mathbf{r} - \mathbf{r}_i|}{v}, \tag{5}$$

where v is the wave propagation velocity in the medium.

We define a 3-D grid of assumed source positions, broad enough to include the actual source. Traveltimes τ_i' from every grid to every receiver are calculated using eq. (5). The calculation of the arrival times τ_i using eq. (4), however, requires a knowledge of the event origin time t_0. Since t_0 is unknown, we select a certain time t_w as the beginning of an M-sample-long window containing the signal of interest. For each assumed source position, the origin time of the event contained in the window is taken as

$$t_0(\mathbf{r}) = t_w - \min[\tau_i'(\mathbf{r})]. \tag{6}$$

The application of eq. (2) yields a 3-D distribution of semblance $S(\mathbf{r})$ whose maximum identifies the most likely position of the source of the waves contained in the analysis window.

This procedure is repeated by sliding the analysis window along the signal. In this way we compute a series of spatial distributions of semblance corresponding to different time windows spanning the interval from the pre-event noise to the coda. To obtain a unique solution

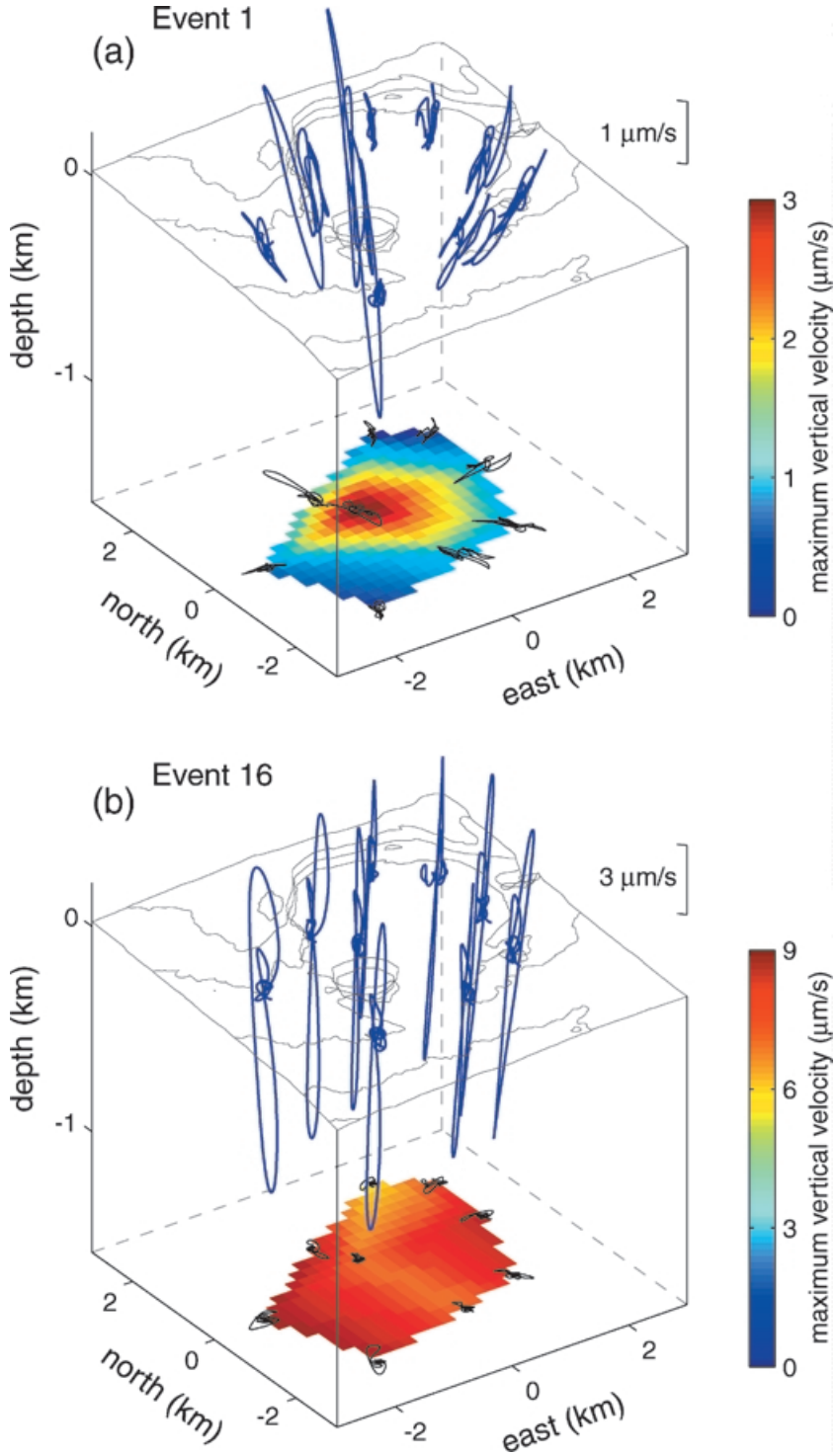

Figure 3. Particle motions (in blue) in a 40-s window centered on the VLP signal for (a) Event 1 and (b) Event 16. The particle motions are plotted at the corresponding station locations. Horizontal projections of the particle motions (in black) are shown at the base of the cube. The colour maps at the base of the cube represent the maximum vertical amplitude of ground velocity plotted as a function of spatial location on the caldera and are obtained by applying a 2-D linear gridding algorithm to the maximum VLP amplitudes recorded at each station of the network.

and enhance the stability of this solution, we define an average semblance distribution for the event. This distribution is obtained by selecting those semblance distributions whose peak semblance is higher than 90 per cent of the absolute maximum obtained in all windows, and averaging the corresponding values of semblance separately at each grid node. A source location and error region can be defined respectively as the position where the average semblance reaches its maximum and the subset of grid nodes where the average semblance is higher than a certain value. For example, Ohminato *et al.* (1998) and Chouet *et al.* (1999) used 97 per cent of the maximum semblance to define the error limits in their source locations. This definition is too conservative to be applied as a general rule. Detailed studies of the performance of the

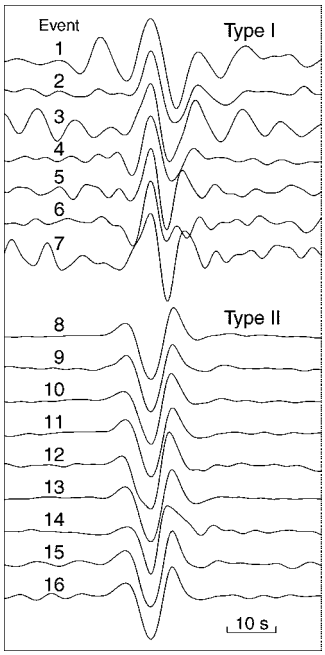

Figure 4. Normalized vertical component velocity seismograms recorded at station NPB for the 16 events selected. The traces are filtered between 8 and 60 s to extract the VLP signals. Type I and Type II events are plotted separately. The numbers at the left refer to the event number in Table 1.

semblance method (Almendros *et al.*, in preparation) suggest that the use of a range of values according to the quality of the signals may be more appropriate to define location errors.

5 DATA ANALYSIS AND RESULTS

For each event, we extract 300 s of data centred on the VLP signal and bandpass filter the traces in a 10–20 s band centered on the spectral maximum. Semblance calculations are then performed in a 25 s long window sliding in increments of 5 s along the traces. We use a constant P-wave velocity $v = 4$ km s^{-1}, which represents an average velocity in the top layers of the tomographic model obtained by Dawson *et al.* (1999) for Kilauea Volcano. Our grid search domain consists of $51 \times 51 \times 51$ nodes with cell size of $200 \times 200 \times 200$ m and extends from -5 to 5 km in the east–west direction, from -5 to 5 km in the north–south direction, and from 0 to 10 km in depth. The origin of the coordinate system is fixed at 19°24.5′N, 155°17.0°W, at an elevation of 1088 m above sea level (the average elevation of the caldera floor). The source location is defined as the grid node where the average semblance distribution reaches its maximum. Error limits are defined by the region within which the average semblance is above a certain level. The selection of this level is based on the quality of the signals. Type I events have average signal-to-noise ratios in the range 2–3, and we select the top 3 per cent of the average semblance distributions to define their error limits. For Type II events, with signal-to-noise ratios around 6–10, the error region is defined by the top 1 per cent of the average semblance distributions. When the location errors are much larger than the grid cell size, no better constraint of the source location can be obtained by using a finer grid. For errors on the order of the grid size, we refine the location by repeating the semblance calculations over a smaller domain with the same number of nodes and origin but with a smaller cell size of $40 \times 40 \times 40$ m.

Fig. 5 shows examples of results for Event 1 (Type I) and Event 16 (Type II). High values of peak semblance are generally reached in time windows centered around the pulses and low peak semblance values are obtained for windows containing mainly noise. Locations are stable for a few tens of seconds in the high-semblance windows. The source locations of the 16 VLP signals determined by this method are listed in Table 1 and are illustrated in Fig. 6.

6 DISCUSSION

Source locations for events of Types I and II are spatially distinct. All the sources of Type I events are located at shallow depths (∼1 km) beneath the northeast edge of the Halemaumau pit crater, in close proximity to the sources previously imaged by Chouet & Dawson (1997) and Ohminato *et al.* (1998). The sources of Type II events are located near 8 km depth below the northwest quadrant of Kilauea caldera, except for one event located at ∼6 km depth.

Several authors have addressed the issue of contamination of VLP signals by tilt (Wielandt & Forbriger 1999; Hidayat *et al.* 2000). Tilt effects may affect horizontal components measured in the near field, where they can introduce distortions in the apparent directions of observed particle motions, thereby producing a bias in the estimated source depths. To assess whether spurious tilt effects may be present in our signals, we underscore the following facts. First, recall that the directions of particle motion are not the only evidence that points to distinct source depths for Type I and Type II events. As shown in Fig. 3, the spatial attenuation patterns of signal amplitudes are different

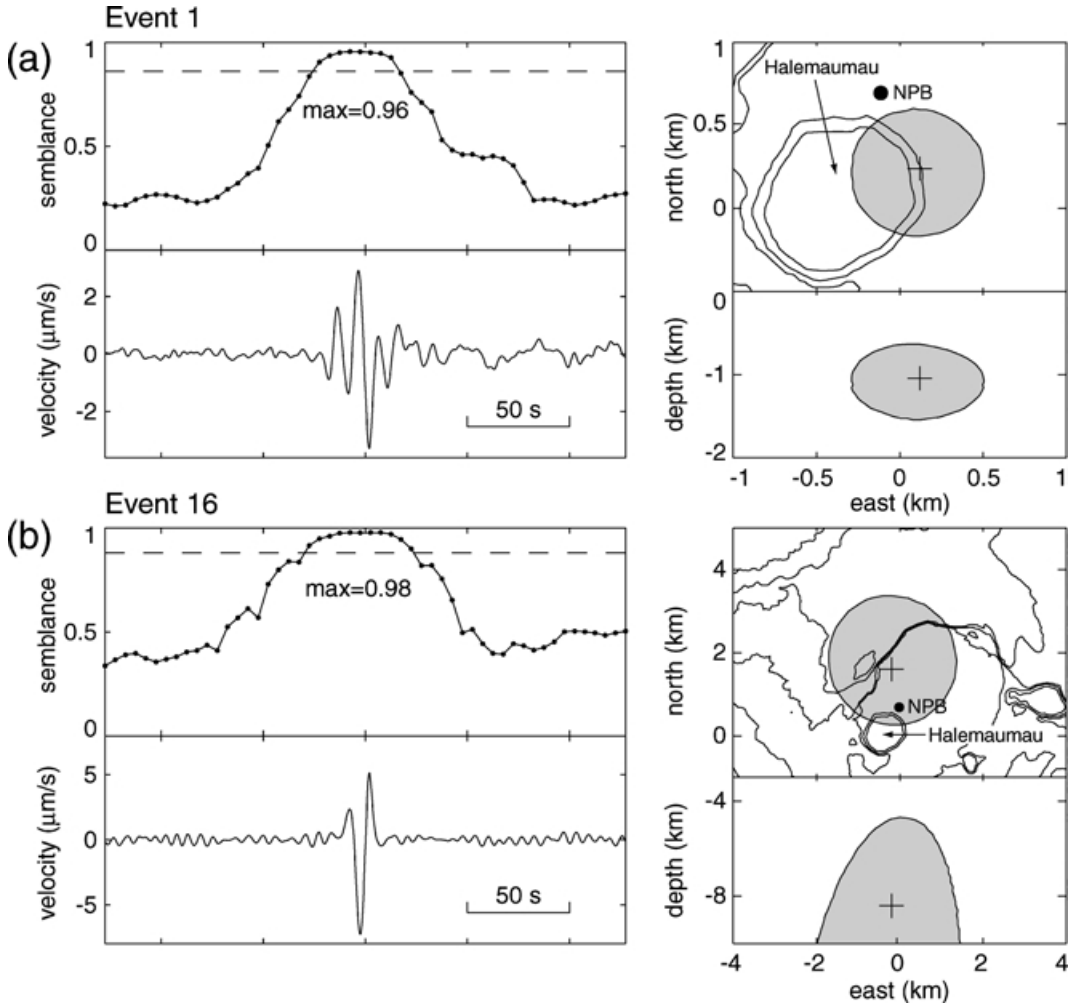

Figure 5. Source locations obtained by the average semblance method for (a) Event 1 and (b) Event 16. The top left panel in each figure shows the peak semblance obtained for different windows along the signal. The dashed line represents 90 per cent of the absolute maximum of semblance, identified by the label *max*. All semblance distributions with peak semblances above this level are stacked to obtain the average semblance distribution used to define the source location. The bottom left panel shows the vertical component velocity seismogram at station NPB. The two panels at the right show a map view and an east–west vertical cross-section of the medium across the source position represented by a cross. The shaded area shows the size of the error region (see text for explanations).

for each type of event, leaving little doubt that the source depths for Type II events are deeper than those for Type I events. Second, Type II events at all stations, and Type I events at stations closest to the source region, are dominated by vertical motions which are not affected by tilt. If there was a tilt effect at these stations, then the spurious tilt signal would have to compensate exactly translational horizontal motions at all stations, a highly unlikely condition in our view. As a final test, we used synthetic calculations to determine whether an important bias might have been introduced in our results by spurious horizontal displacements due to tilting of the sensors. Free surface displacements and rotations generated by isotropic sources embedded at different depths under Halemaumau were calculated separately at each receiver location in our network. In all our models, we used a fixed source–time function in the form of a Ricker wavelet with period of 15 s, comparable to the dominant period observed in our VLP signals (see Fig. 2), and selected moment tensor magnitudes adequate to reproduce the average amplitude observed at station NPB for Type I and Type II signals. Our numerical results demonstrate that apparent displacements induced by rotation are only measurable on horizontal components for surficial sources, and that such displacements produce a decrease in rectilinearity rather than a change in the orientation of particle motions. Based on these considerations, we conclude that our data are not biased by tilt effects.

At present, it is not possible to elucidate the actual shape of the conduit and to assess whether or not the sources of Type I and Type II events imaged in Fig. 6 are part of the same conduit. If one assumes that both source regions are spatially connected by a linear conduit, then this conduit would dip $\sim 80^{\circ}$ to the north from the northeast side of Halemaumau toward Uwekahuna Bluff. The similarities in VLP waveforms and characteristics observed for both Type I and Type II events suggest the repetitive action of non-destructive sources. In spite of their deeper origins, Type II events display larger amplitudes than those observed for Type I events. For example, at station NPB the average radial amplitude of Type II events is four times larger than the average radial amplitude of Type I events. Taking into account the strong

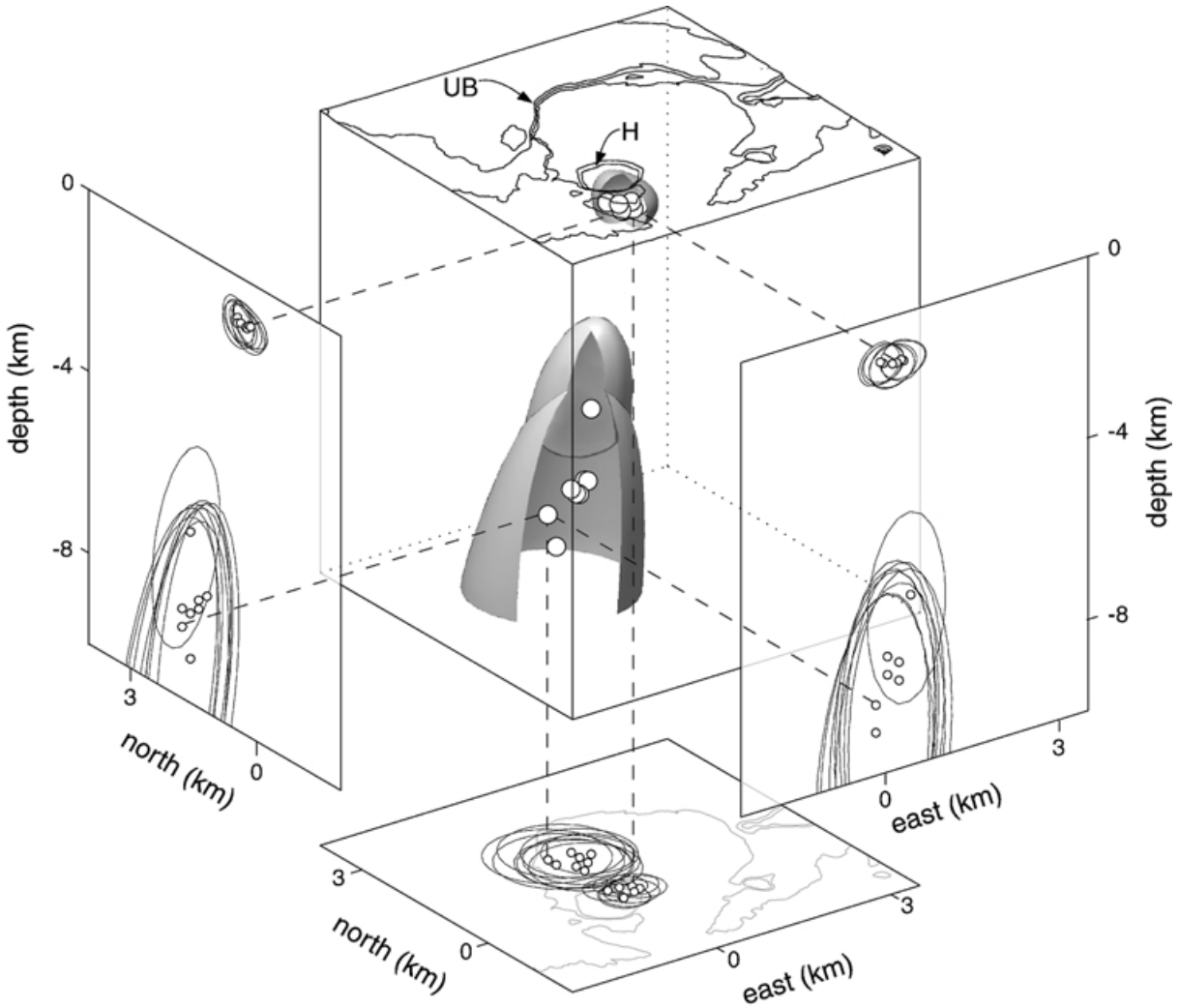

Figure 6. Source locations of the 16 events analyzed in this paper (large open circles). The topography of Kilauea caldera is shown at the top of the domain to help identify the locations of the VLP sources within the volcanic edifice (H = Halemaumau, UB = Uwekahuna Bluff). Small open circles mark the projections of the source locations on the sides and bottom of the volume shown. Contours on the side planes are projections of the error regions for the source locations. Dashed lines identify the locations of Events 1 and 16 depicted in Figs 2, 3, and 5. Topographic contours are shown on the bottom projection for a better view of the source locations in relation to caldera features. The grey surfaces represent the outline of the error regions for all events.

attenuation of the near-field components with distance ($\sim r^{-3}$), the amplitude of elastic radiation in the deeper sources is over 2000 times larger than that in the shallow sources, which may reflect the scaling of pressure with depth and/or larger dimensions for the deeper sources.

Several studies address the location and analysis of VLP signals in volcanoes. Location techniques vary, ranging from simple intersections of particle motion (e.g. Rowe *et al.* 1998), to semblance locations (Matsubayashi 1995; Chouet *et al.* 1999; Kawakatsu *et al.* 2000), to refined positioning based on a minimization of residual errors between observed waveforms and synthetics in moment tensor inversions (Ohminato *et al.* 1998; Legrand *et al.* 2000; Nishimura *et al.* 2000). For example, Kawakatsu *et al.* (2000) located VLP sources between 1.0 and 1.5 km beneath Aso Volcano, and Hidayat *et al.* (2000) documented VLP signals located only 100 m beneath the summit dome of Merapi Volcano. Chouet *et al.* (1999) studied VLP pulses associated with Strombolian explosions at Stromboli Volcano and inferred a source depth of 300 m beneath the active vents. Nishimura *et al.* (2000) located VLP signals at about 2 km beneath Iwate Volcano; Rowe *et al.* (1998) reported on the occurrence of VLP signals at depths of several hundred metres beneath Erebus Volcano; and Arciniega-Ceballos *et al.* (1999) postulated a shallow VLP source located a few kilometres below Popocatepetl Volcano. Based on the often-observed temporal coincidence of VLP signals and eruptive behavior, most studies propose that an interaction between the flow of magma and slugs of magmatic gases is the most likely mechanism to explain the generation of seismic energy in the VLP band (Uhira & Takeo 1994; Ohminato *et al.* 1998; Rowe *et al.* 1998; Chouet *et al.* 1999; Hidayat *et al.* 2000). Source mechanisms involving hot water and/or mud have also been found to be viable to explain phreatic eruptions at Aso Volcano (Kaneshima *et al.* 1996; Kawakatsu *et al.* 2000).

At Kilauea, previous analyses of VLP signals by Chouet & Dawson (1997) and Ohminato *et al.* (1998) detected the presence of shallow sources located at depths near 1 km beneath the northeast edge of Halemaumau. The source mechanisms determined by these authors identify cracks with different orientations, leading to an interpretation of this source region as a plexus of cracks. Our locations for Type I events

coincide with the source positions obtained by Chouet & Dawson (1997) and Ohminato *et al.* (1998), however the VLP signatures are different, which is again suggestive of different source mechanisms. The repeated occurrence of shallow VLP events in the same region during the period from 1996 to 1999 thus appears to be consistent with recurrent excitations of a temporally stable plexus of cracks by unsteady fluid flow.

Two types of fluids may be considered at the source of the shallow VLP signals recorded at Kilauea, namely magmatic or hydrothermal fluids. The implications of the presence of a magmatic versus hydrothermal environment at depths of ∼1 km beneath Kilauea caldera are different. If the fluid is magma, then the present assumption concerning the structure of the shallow plumbing system of Kilauea should be revised to account for the observation that magma rises to very shallow depths before branching into the East Rift zone to feed the ongoing eruption at Puu Oo, which began in January 1983. The working assumption usually applied at Kilauea is that seismic energy generated from sources shallower than 2 or 3 km must be reflecting hydrothermal activity, mainly because these depths are thought to represent the upper limit of the magma reservoir as inferred from voids in the distribution of hypocenters of VT earthquakes at depths between 2 and 7 km below the caldera floor (Ryan *et al.* 1981; Klein *et al.* 1987). Several recent observations, however, are at odds with this view. For example, constraints on the spatial extent of the hydrothermal system beneath the Kilauea summit were obtained from array analyses of shallow long-period seismicity in Kilauea caldera (Almendros *et al.* 2001). These analyses reveal the presence of an active hydrothermal system extending to a depth of 500 m beneath the northeast edge of Halemaumau, and point to a lack of hydrothermal activity below that level. Therefore, the generation of VLP signals by hydrothermal fluids at depths larger than 500 m is unlikely.

A more plausible explanation for the generation of VLP signals at ∼1 km depth involves a magmatic origin. Evidence for the presence of magma at shallow depths is provided by recent tomographic studies (Okubo *et al.* 1997; Rowan & Clayton 1993; Dawson *et al.* 1999). These studies reveal the presence of low-velocity and V_P/V_S anomalies, which are generally interpreted as indicative of the presence of partial melt, at depths shallower than a few kilometres. Based on the model of Takei (2001), we infer that the volume fraction of melt associated with the maximum anomalies may range from 4 to 14 per cent, and may be distributed in small pockets of magma embedded in a hot rock rather than in a single magma chamber. The low-velocity anomalies are not spatially correlated with aseismic zones, in contradiction to the aseismic assumption used to define the position and spatial extent of the summit magma reservoir. The shallow structure imaged using traveltime tomography thus appears to be inconsistent with the current model of the plumbing system. Robust evidence for the presence of magma in a shallow conduit beneath Halemaumau also comes from a study by Ohminato *et al.* (1998), who analyzed VLP signals associated with a magmatic surge at Puu Oo in 1996. On February 1, 1996, a 22 μrad summit inflation in response to the injection of magma under Kilauea caldera was accompanied by sawtooth VLP displacement signals characterized by a 2–3 min rise phase followed by a 5–10 s drop phase (Dawson *et al.* 1998; Ohminato *et al.* 1998). Ohminato *et al.* (1998) located the source of these signals at a depth of 1 km beneath the northeast edge of Halemaumau. They performed waveform inversions of the VLP signals and imaged a source mechanism consisting of a sill-like conduit, which slowly inflates as it fills with magma and gas, and suddenly deflates with the release of the two-phase fluid through the crack outlet. Ohminato *et al.* (1998) also found that the time-integrated volume change at the VLP source was consistent with the volume of lava produced at the eruptive site down rift. At the time, these results were interpreted as an isolated episode not reflecting the normal state of the volcano. However, the recurrent detection of VLP signals in the same source region since 1996, documented in Chouet & Dawson (1997) and in the present paper, is strongly suggestive of a sustained injection of magma through the same permanent plexus of cracks.

Studies of VLP signals done so far share a common result in that they all point to shallow sources (Uhira & Takeo 1994; Ohminato *et al.* 1998; Rowe *et al.* 1998; Chouet *et al.* 1999; Kawakatsu *et al.* 2000; Hidayat *et al.* 2000). The present paper, however, documents the occurrence of a different type of VLP events with source depths ∼ 8 km. Although the source mechanisms of these deeper events are unknown, we surmise that these signals originate in transients in the flow of magma in a manner similar to the transients occurring in the shallow sources identified earlier (Chouet & Dawson 1997; Ohminato *et al.* 1998). This represents the first time that such deep VLP signals have been identified under Kilauea or elsewhere, and opens up the possibility of imaging magma conduits beneath volcanoes deeper than imagined before by locating the different segments of conduit that generate VLP signals. Two conditions are necessary for a successful completion of such a task: first, long-term observations to enable the detection of a sufficient number of VLP signals from a variety of sources along the conduit; and second, large-aperture seismic networks to enable precise locations for the deeper portions of the plumbing system.

ACKNOWLEDGMENTS

We thank Fred Klein, Wayne Thatcher, Robert Tilling, Torsten Dahm and an anonymous reviewer for their constructive comments. Javier Almendros was supported by a Fellowship of the Spanish Ministry of Education.

REFERENCES

Almendros, J., Chouet, B. & Dawson, P., 2001. Spatial extent of a hydrothermal system at Kilauea Volcano, Hawaii, determined from array analyses of shallow long-period seismicity, 2. Results, *J. geophys. Res.,* **106,** 13 581–13 598.

Arciniega-Ceballos, A., Chouet, B. & Dawson, P., 1999. Very long period signals associated with vulcanian explosions at Popocatepetl Volcano, Mexico, *Geophys. Res. Lett.,* **26,** 3013–3016.

Aster, R., Lees, J. & Neuberg, J. (eds), 2000. Broadband seismic and acoustic observations of volcanic seismicity, *J. Volc. Geotherm. Res.,* **101** (special issue), vii–viii.

Chouet, B., 1996a. Long-period volcano seismicity: its source and use in eruption forecasting, *Nature,* **380,** 309–316.

Chouet, B., 1996b. New methods and future trends in seismological volcano monitoring, in *Monitoring and mitigation of volcano hazards,* eds Scarpa, R. & Tilling, R., pp. 23–97, Springer-Verlag, Berlin.

Chouet, B.A. & Dawson, P.B., 1997. Observations of very-long-period impulsive signals accompaying summit inflation at Kilauea Volcano, Hawaii, in February 1997, (abstract), *EOS, Trans. Am. geophys. Un.,* **76,** Fall Meeting Suppl., S11C-3.

Chouet, B., Saccorotti, G., Dawson, P., Martini, M., De Luca, G., Milana, G. & Cattaneo, M., 1999. Broadband measurements of the sources of explosions at Stromboli Volcano, Italy, *Geophys. Res. Lett.,* **26,** 1937–1940.

Dawson, P., Dietel, C., Chouet, B., Honma, K., Ohminato, T. & Okubo, P., 1998. A digitally telemetered broadband seismic network at Kilauea Volcano, Hawaii, *US Geol. Surv. Open-file Report,* **98-108,** 122.

Dawson, P., Chouet, B., Okubo, P., Villaseñor, A. & Benz, H., 1999. Three-dimensional velocity structure of the Kilauea caldera, Hawaii, *Geophys. Res. Lett.,* **26,** 2805–2808.

Falsaperla, S., Langer, H., Martinelli, B. & Schick, R., 1994. Seismic measurements on Stromboli Volcano in a wide frequency range, *Acta Vulcanol.,* **5,** 173–178.

Heliker, C., Mangan, M., Mattox, M., Kauahikaua, J. & Helz, R., 1998. The character of long-term eruptions: inferences from episodes 50–53 of the Puu Oo-Kupaianaha eruption of Kilauea Volcano, *Bull. Volc.,* **59,** 381–393.

Hidayat, D., Voight, B., Langston, C., Ratdomopurbo, A. & Ebeling, C., 2000. Broadband seismic experiment at Merapi Volcano, Java, Indonesia: very-long-period pulses embedded in multiphase earthquakes, *J. Volc. Geotherm. Res.,* **100,** 215–231.

Julian, B.R., 1994. Volcanic tremor: nonlinear excitation by fluid flow, *J. geophys. Res.,* **99,** 11 859–11 877.

Kaneshima, S. *et al.*, 1996. Mechanism of phreatic eruptions at Aso Volcano inferred from near-field broadband seismic observations, *Science,* **273,** 642–645.

Kawakatsu, H. *et al.*, 2000. Aso94: Aso seismic observation with broadband instruments, *J. Volc. Geotherm. Res.,* **101,** 129–154.

Klein, F.W., Koyanagi, R.Y., Nakata, J.S. & Tanigawa, W.R., 1987. The seismicity of Kilauea's magma system, in *Volcanism in Hawaii,* eds Decker, R.W., Wright, T.L. & Stauffer, P.H., pp. 1019–1085, USGS Prof. Paper 1350.

Kumagai, H., Ohminato, T., Nakano, M., Ooi, M., Kubo, A. & Inove, H., 2001. Very-long-period seismic signals and caldera formation at Miyake Island, Japan, *Science,* **293,** 687–690.

Lahr, J.C., Chouet, B.A., Stephens, C.D., Power, J.A. & Page, R.A., 1994. Earthquake classification, location and error analysis in a volcanic environment: implications for the magmatic system of the 1989–1990 eruptions at Redoubt Volcano, Alaska, *J. Volc. Geotherm. Res.,* **62,** 137–151.

Legrand, D., Kaneshima, S. & Kawakatsu, H., 2000. Moment tensor analysis of near-field broadband waveforms observed at Aso Volcano, Japan, *J. Volc. Geotherm. Res.,* **101,** 155–169.

Matsubayashi, H., 1995. Origin of the long-period tremors and long-period seismic waves preceding mud eruptions observed at Aso Volcano (in Japanese), *MSc thesis,* University of Tokyo, Tokyo.

Neidel, N. & Tarner, T., 1971. Semblance and other coherency measures for multichannel data, *Geophysics,* **36,** 482–497.

Neuberg, J., Luckett, R., Ripepe, M. & Braun, T., 1994. Highlights from a seismic broadband array on Stromboli Volcano, *Geophys. Res. Lett.,* **21,** 749–752.

Nishimura, T. *et al.*, 2000. Source process of very long period seismic events associated with the 1998 activity of Iwate Volcano, northeastern Japan, *J. geophys. Res.,* **105,** 19 135–19 147.

Ohminato, T., Chouet, B., Dawson, P. & Kedar, S., 1998. Waveform inversion of very long period impulsive signals associated with magmatic injection beneath Kilauea Volcano, Hawaii, *J. geophys. Res.,* **103,** 23 839–23 862.

Okubo, P., Benz, H. & Chouet, B., 1997. Imaging the crustal magma sources beneath Mauna Loa and Kilauea Volcanoes, Hawaii, *Geology,* **25,** 867–870.

Rowan, L.R. & Clayton, R.W., 1993. The three-dimensional structure of Kilauea Volcano, Hawaii, from travel time tomography, *J. geophys. Res.,* **98,** 4355–4375.

Rowe, C.A., Aster, R.C., Kyle, P.R., Schlue, J.W. & Dibble, R.R., 1998. Broadband recording of Strombolian explosions and associated very-long-period seismic signals on Mount Erebus Volcano, Ross Island, Antarctica, *Geophys. Res. Lett.,* **25,** 2297–2300.

Ryan, M.P., Koyanagi, R.Y. & Fiske, R.S., 1981. Modeling of the three-dimensional structure of macroscopic magma transport system: application to Kilauea Volcano, Hawaii, *J. geophys. Res.,* **86,** 7111–7129.

Takei, Y., 2001. Effect of pore geometry on V_P/V_S: a continuous view from equilibrium geometry to crack, *J. geophys. Res.,* submitted.

Uhira, K. & Takeo, M., 1994. The source of explosive eruptions of Sakurajima Volcano, Japan, *J. geophys. Res.,* **99,** 17 775–17 789.

Wassermann, J., 1997. Locating the sources of volcanic explosions and volcanic tremor at Stromboli Volcano (Italy) using beam-forming on diffraction hyperboloids, *Phys. Earth Planet. Int.,* **104,** 271–281.

Wielandt, E. & Forbriger, T., 1999. Near-field seismic displacement and tilt associated with the explosive activity of Stromboli, *Ann. Geophys.,* **42,** 407–416.